Metal-insulator transitions and singlet polarons in one-dimensional $Ca_{2+x}Y_{2-x}Cu_5O_{10}$

A. Filippetti and V. Fiorentini
CNR-INFM-SLACS and Dipartimento di Fisica, Università di Cagliari, Monserrato, I-09042 Cagliari, Italy
(Received 16 April 2008; revised manuscript received 29 May 2008; published 27 June 2008)

One-dimensional dopable $Ca_{2+x}Y_{2-x}Cu_5O_{10}$ is characterized by the presence of Zhang-Rice singlets (ZRSs) in the electronic ground state and a series of magnetic and metal-insulating phase transitions. With the use of unconventional first-principles calculations suited to the study of strongly correlated materials, we describe the change in the electronic and magnetic properties through the whole doping range (up to one hole per CuO_2 unit). Singlet polarons, whose space and energy distributions are described in detail, are found by our calculations to be stable above a concentration of ~0.3 holes per Cu. We give a sound interpretation of the observed insulating behavior and loss of antiferromagnetic ordering at low doping and predict unusual properties in the doping region, where experimental data are not yet available. The system is antiferromagnetic and hopping conducting for x/n up to about 0.25, gapped around 0.3–0.4, metallic from 0.4 to 1, and gapped and ZRS-saturated at $x/n=1$.

DOI: 10.1103/PhysRevB.77.235124 PACS number(s): 74.25.Jb, 71.30.+h, 74.20.−z, 74.72.−h

I. INTRODUCTION

The long-time interest in one-dimensional cuprates is primarily motivated by the need to uncover the fundamental mechanisms lying at the basis of high-T_c superconductivity.[1,2] Their wide array of unconventional properties (e.g., spin-charge separation, Peierls instabilities, non-Fermi-liquid behavior, and polaron formation), possibly but not necessarily related to superconductivity, have further increased their unique appeal. If these were not enough, highly nonlinear optical properties also suggest possible applications of one-dimensional cuprates in microelectronics as components of ultrafast optical-switching devices.[3,4]

As for the electronic properties, the presence of singlet polarons, commonly known as Zhang-Rice singlets (ZRSs) in the framework of bidimensional high-T_c superconducting cuprates (and first described through a single-band effective Hamiltonian by Zhang and Rice[5] in 1988 after the original suggestion of Anderson[2]), is unquestionably the most distinctive trait of many doped (or even self-doped) cuprates. In one-dimensional cuprates this presence is even more emphasized as the Cu *d* Coulomb repulsion, which is the driving forces of ZRS formation, is maximized. Also, one dimensionality is welcomed by experimentalists and theoreticians alike as, on the one hand, it simplifies the disentanglement of electronic and structural properties, and on the other hand, it allows simpler structural modeling and generally less expensive computing tasks.

Unfortunately, certified one-dimensional cuprates are not so abundant. Known systems built on aggregation of weakly coupled chains (or ladders) of CuO_2 units are $GeCuO_3$, Li_2CuO_2, $SrCuO_2$, Sr_2CuO_3, and $Sr_{14}Cu_{24}O_{41}$, but for these compounds attempt to introduce doping in meaningful amount has failed so far (except for $Sr_{14}Cu_{24}O_{41}$ that can be doped by Sr-Ca substitutions, but its overly complicated structure hinders a clear understanding of the fundamental mechanisms).

In this respect, $Ca_{2+x}Y_{2-x}Cu_5O_{10}$ (CaYCuO in the following), whose solid solution was synthesized for the first time by Hayashi *et al.*[6] in 1998, is a remarkable exception; it is made of a simple assembly of weakly coupled CuO_2 zigzag chains intercalated by parallel-running chains of Ca/Y mixture merely acting as positive (i.e., hole) charge reservoir for the CuO_2 units (see Fig. 1). At variance with more complicated cuprates, such as $YBa_2Cu_3O_{6+x}$, where CuO_2 layers and CuO_x chains dispute possession of the holes, here any Y-to-Ca substitution must inject a single hole within the CuO_2 stripes. The relative Ca and Y concentrations can be controlled in a wide interval, thus making this system an ideal prototype of dopable one-dimensional cuprates. Also,

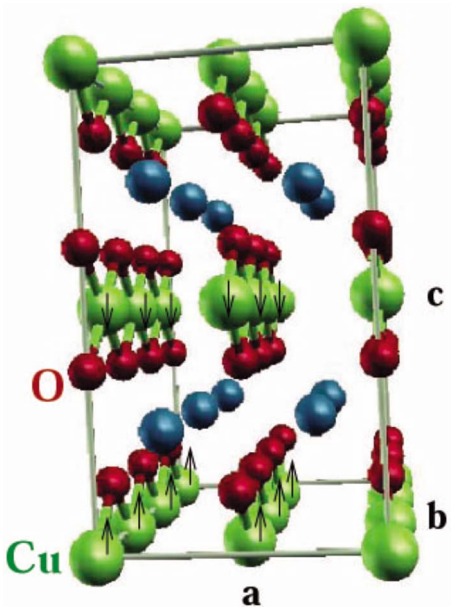

FIG. 1. (Color online) Structure of CaYCuO made of FM Cu chains parallel to the *y* direction. The dashed lines draw the orthorhombic AF unit cell with $n=3$ (i.e., three Cu per unit chain, see text). The contiguous chains are weakly AF coupled along *c*, while coupling along *a* is discardable. The intercalated chains of Ca/Y mixture run parallel to the CuO_2 chains, acting exclusively as electron reservoir for the CuO_2 units. CuO_2 chains located at $(0,y,0)$ and $(1/2,y,1/2)$ are shifted along *y* by half Cu-Cu distance with respect to chains $(1/2,y,0)$ and $(0,y,1/2)$.

neutron-diffraction experiments[7] show that the undoped compound presents weak intrachain ferromagnetic (FM) ordering (chains run parallel to the b axis in Fig. 1) and minimal interchain couplings that are antiferromagnetic (AF) along c and FM along a, so the system is overall a-type AF with T_N=29.5 K. The intrachain FM ordering avoids the complicacy of spin-Peierls dimerization found, e.g., in $GeCuO_3$.

From the change in magnetic and conducting properties measured in the doping range $x=[0,2]$ or $x/n=[0,0.4]$ (here x is the hole concentration of the unit chain, $n=5$ is the number of CuO_2 chain steps in the unit chain, and x/n is the hole fraction per CuO_2 unit), experiments[6–9] infer that in a well-defined doping range this compound must be highly populated by ZRS. From the undoped Mott-insulating AF phase at low doping ($x/n<0.25-0.3$), the systems become an AF insulator with conductivity $\sigma \sim \exp(T^{-1/2})$ typical of one-dimensional hopping conduction. In this region the AF susceptibility is well described by the Curie-Weiss behavior with T_N due to the small z-parallel interchain coupling smoothly decreasing from 28 K at zero doping to 16 K at $x/n=0.2$. At $x/n \sim 0.3$ the system undergoes a phase transition to a ZRS-rich phase, where magnetic ordering is lost and the AF susceptibility peak at T_N spreads out in a broad maximum. This is a typical signature of magnetic chains populated by a high density of singlets making a transition to a spin-glass (or spin-liquid) phase. Intriguingly, the system remains substantially insulating even up to a rather large (i.e., $x/n \sim 0.4$) hole doping concentration, and indeed a thermally activated conduction ($\sigma \sim \exp(-E_{gap}/k_BT)$ across a gap $E_{gap} \sim 0.08$ eV is reported.[6] It is perhaps unexpected that injected holes do not lead to conductivity (i.e., they remain spatially localized) up to such a large doping (in comparison $Y_{1-x}Ca_xBa_2Cu_3O_6$ is reportedly metallic for $x/n>0.1-0.15$ when superconductivity appears). No data are available, to our knowledge, for concentrations above $x/n=0.4$.

From these observations, the system appears as an ideal benchmark to prove the general capability of a theory to describe the presence and the effects of ZRS and magnetic polarons in general. So far, the theoretical description of ZRS has been an exclusive matter of model Hamiltonians of the Hubbard type or close variants thereof, such as the aforementioned Zhang-Rice Hamiltonian,[5] which integrates out the oxygen degrees of freedom and assumes the large U limit, becoming only dependent on the hopping (t) and exchange (J) parameters of a single band (see also Refs. 10 and 11). While this may capture the essential physics of these materials, it forgoes the detailed description of the electronic properties. Furthermore, models are applied to fictitious geometries, such as single CuO_2 units, but the detailed knowledge of structural and electronic properties is generally essential to understand the behavior of real materials. For this aim, first-principles calculations are the most valuable approach in principle. In practice though, conventional first-principles methodologies (e.g., the local-spin-density approximation to density-functional theory or LSDA) are known to be inadequate to describe strongly correlated systems, so theoreticians have to rely on beyond-LSDA approaches that are usually hard to implement and computationally awe inspiring.

In previous papers[12–17] we have shown that fully *ab initio* calculations based on the pseudo-self-interaction correction (PSIC) approach[12] can, in fact, accurately describe the fundamental quantum chemistry of several strongly correlated electrons and doped copper oxides, in particular. Here we furnish an important addiction to the successful performance of the PSIC, that is, the description of ZRS formation in doped CaYCuO in terms of a transparent band energy picture. In our supercell approach doping can be introduced in a realistic manner with the use of large cells, and the ZRS morphology in a realistic three-dimensional representation within real materials, as well as the effects on magnetic and conducting properties, is examined, providing a detailed account of the microscopic properties of CaYCuO through the whole doping concentration range $x/n=[0,1]$.

II. METHOD

Calculations based on LSDA or the generalized gradient approximation are unapplicable to insulating cuprates as they fail to reproduce the spin-polarized ground state ($S=1/2$) of the Cu^{2+} ion. As a consequence, magnetic insulating cuprates are usually described as nonmagnetic metals. This failure is related to the presence of the spurious self-interaction (SI) in the single-particle equations, i.e., the unphysical interaction of a charge with its own generated potential. Due to the SI, any d state, whether empty or occupied, is subject to the Coulomb repulsion of the nine electrons of the Cu^{2+} d^9 shell; thus, no energy gap can open within the d manifold. To overcome the problem, the PSIC approach[12] includes in the LSDA potential an atomiclike contribution that eliminates the SI effects without compromising the affordable computational cost and overall simplicity of the LSDA scheme (in particular the PSIC single-particle potential is not explicitly state dependent as in the full SIC approach[18] whose state dependence may cause serious trouble[19]). Since the PSIC does not imply a major increase in the computational effort compared to the standard LSDA, we can include doping (even at low concentration) in a realistic manner, i.e., with real atomic substitutions in large supercells, avoiding virtual-crystal approximations. With respect to the (similar in several aspects) LDA+U approach, the PSIC has the advantage of being independent of the parameter choice and more generally applicable to insulators, metal, magnetic, and nonmagnetic systems alike (see Ref. 12 for a detailed discussion).

Our single-particle Hamiltonian is solved in a computational framework based on plane-wave basis set and ultrasoft pseudopotentials[20] with a cutoff energy of 30 Ry. Reciprocal-space k-point grids of $2\times12\times2$, $10\times10\times10$, and $11\times11\times11$ were used for self-consistent solutions, density of states (interpolated through linear tetrahedron method), and Fermi-surface calculations, respectively.

We can explore different magnetic and orbital configurations by solving our self-consistent Hamiltonian with suitable starting spin densities corresponding to a given magnetic configuration and then letting the system relax self-consistently to a local minimum. If different magnetic solutions for the same doping concentration are obtained, the one with the lowest total energy is the ground state, while the

TABLE I. Energy gap (eV) and magnetization $M(\mu_B)$ calculated within PSIC in comparison with experimental values (in parentheses, if available).

	CaYCuO	CuO	$GeCuO_3$	$YBa_2Cu_3O_6$
E_{gap} (eV)	3.44	2.2 (1.7)	3.34 (3.7)	1.45 (1.5)
$M(\mu_B)$	0.71 (0.9)	0.72 (0.68)	0.77 (0.7)	0.55 (0.5)

others can be interpreted as magnetic excitations.

The structure of CaYCuO, reported in Fig. 1, is an assembly[6–8] of weakly interacting CuO_2 FM zigzag chains with Cu-Cu separation of 3.4 Å and Cu-O-Cu angle of $\sim 90°$. CuO_2 chains located at $(0,y,0)$ and $(1/2,y,1/2)$ are shifted along the b axis by half Cu-Cu distance with respect to the chains at $(1/2,y,0)$ and $(0,y,1/2)$. In our calculations the chains are oriented along the b axis (i.e., the y direction), with Cu-O bonds lying within the (b,c) plane. We assume the experimental lattice parameters[7] $a=6.172$ Å, $b/n=2.811$ Å, and $c=10.572$ Å.

Notice that the ratio of Ca/Y and CuO_2 chain steps is rational. In the unit cell of the synthesized compound, there are $n=5$ chain steps of CuO_2, each of the four steps of Y/Ca, hence the commonly reported formula $Ca_{2+x}Y_{2-x}Cu_5O_{10}$. However for our calculations we assume n as a free parameter to conveniently adapt the chain periodicity to the doping concentration. Indeed, as will be shown explicitly below, the electronic properties depend on x/n, but not on n. In this generalization CuO_2 and Y/Ca steps are in $n/(n-1)$ proportion, and the formula becomes $Ca_{(n-3)+x}Y_{2-x}Cu_nO_{2n}$ [of course, only compositions with $(n-3)+x \geq 0$ can be considered in practice]. In this way we gain a much larger flexibility in selecting the wanted doping concentration through suitable proportion of Y and Ca atoms. In practice we considered $n=2,3,4$ (corresponding to 28-, 44-, and 60-atom unit cells, respectively) and performed calculations through the whole doping range $x/n=[0,1]$ on a dense concentration grid ($\Delta x/n \sim 0.1$).

III. UNDOPED CaYCuO

Undoped CaYCuO is expected to be a prototypical Mott insulator. Our results confirm these expectations. In Table I we report the calculated energy gap and Cu magnetization (values obtained for $n=3$ and $n=4$ are for all purposes identical, confirming that only x or x/n matter, while n does not). We also report values calculated for other prototypical cuprates (CuO, $GeCuO_3$, and $YBa_2Cu_3O_6$ in Refs. 13, 15, and 16, respectively) in comparison with the experiments. These are all charge-transfer AF insulators with energy gap $E_{gap} \sim 1.5-3.5$ eV and Cu magnetization between $0.5\mu_B$ and $1\mu_B$.

Our calculated energy gaps and magnetic moments compare favorably with the experiment, whereas (as explained in Sec. II) LSDA incorrectly predicts metallic nonmagnetic ground states for all these compounds. Furthermore in all cases our calculations predict the correct, i.e., the observed, magnetic ordering as the most energetically stable state with

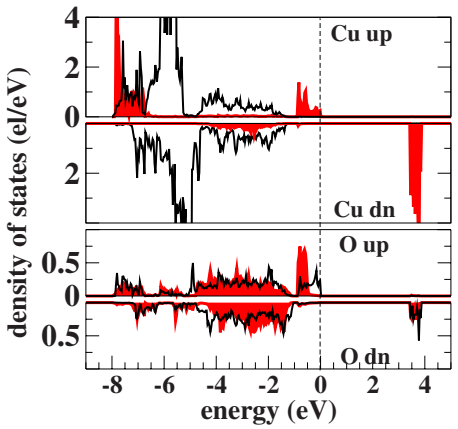

FIG. 2. (Color online) Orbital-resolved DOS of undoped CaYCuO. For Cu the filled (red) area is the contribution of d_{yz} state and the solid line the sum of the other four d orbitals. For O the solid line and filled (red) lines are for p_y and p_z states, respectively.

exchange interaction parameters, in good agreement with available experiments. In particular for CaYCuO we obtain a FM intrachain $J_y=8.46$ meV (compared with ~ 7 meV experimentally) and AF interchain $J_z=-0.2$ meV (~ -1 meV).

In Figs. 2 and 3 we show orbital-resolved density of states (OR-DOS) and band energies for $n=3$ (the same quantities calculated for $n=4$ show no significant differences). The OR-DOS picture shows all the paradigmatic features of the Mott-Hubbard single-band insulating system: coppers are Cu^{2+} (d^9) with the d_{yz} orbital spin polarized, and the corresponding lower (occupied) and higher (empty) Hubbard bands are separated by a nearly atomic U of ~ 11 eV. The gap opens between Cu d_{yz} and O (p_y,p_z) hybrid bands with valence-band top (VBT) and conduction-band bottom having similar orbital characters. This large hybridization, favored by the intrachain FM ordering, induces a sizable magnetization of the oxygens [specifically, nearly 70% magnetization due to Cu d_{yz} and about 15% to each of the two adjacent oxygens (see the $x/n=0$ entry in Table II)].

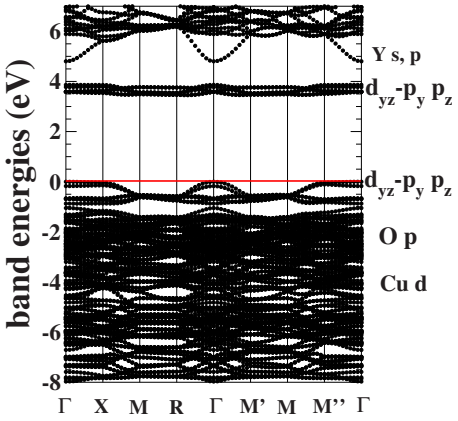

FIG. 3. (Color online) Band energies of undoped CaYCuO within the $n=3$ supercell, which contains 12 Cu atoms. Due to AF symmetry any band in the picture is double degenerate. K points (in crystal coordinates) are $X=[1/2,0,0]$, $M=[1/2,1/2,0]$, $M'=[0,1/2,1/2]$, $M''=[1/2,0,1/2]$, and $R=[1/2,1/2,1/2]$.

TABLE II. Orbital contributions to magnetic moments (in μ_B) and corresponding magnetization of individual CuO_2 units at several x/n doping. If the two oxygens of the same CuO_2 unit are not equivalent, their values are specified in parentheses (e.g., O and O′ for $x/n=1/2$). Atoms labeled with "ZR" are those participating to ZRS, while all the others do not belong to ZRS (the specific atomic locations can be found in the corresponding hole density isosurface plots). At $x/n=7/8$ there are two different kinds of ZRS units corresponding to different ZRS distributions in the chains (for -0-0 and -1-0-, see text).

$x/n=0$	Cu d_{yz}	O p_y	O p_z	CuO_2
	0.70	0.07	0.06	0.96
$x/n=1/4$	Cu d_{yz}	O p_y	O p_z	CuO_2
	0.64	−0.03	0.06	0.70
$x/n=1/3$	Cu d_{yz}	O p_y	O p_z	CuO_2
	0.68	0.08	0.08	1.0
	Cu_{ZR} d_{yz}	$O(O')_{ZR}$ p_y	$O(O')_{ZR}$ p_z	CuO_2
	0.65	0.03(0.06)	−0.68(−0.06)	0.0
$x/n=1/2$	Cu d_{yz}	O p_y	O p_z	CuO_2
	0.61	0.02	0.08	0.81
	Cu_{ZR} d_{yz}	$O(O')_{ZR}$ p_y	$O(O')_{ZR}$ p_z	CuO_2
	0.61	0.02(0.0)	−0.60(−0.16)	−0.13
	Cu′ d_{yz}	O′(O″)p_y	O′(O″)p_z	CuO_2
	0.65	−0.10 (−0.03)	0.05 (0.05)	0.62
$x/n=3/4$	Cu d_{yz}	O p_y	O p_z	CuO_2
	0.62	0.0	0.075	0.70
	Cu_{ZR} d_{yz}	$O(O')_{ZR}$ p_y	$O(O')_{ZR}$ p_z	CuO_2
	0.62	−0.01(0.0)	−0.66(−0.10)	−0.15
$x/n=7/8$	Cu d_{yz}	O p_y	O p_z	CuO_2
	0.62	0.0	0.1	0.82
"-0-0-"	Cu_{ZR} d_{yz}	$O(O')_{ZR}$ p_y	$O(O')_{ZR}$ p_z	CuO_2
	0.62	0.03(0.11)	−0.66(−0.14)	−0.04
"-1-0-"	Cu_{ZR} d_{yz}	$O(O')_{ZR}$ p_y	$O(O')_{ZR}$ p_z	CuO_2
	0.62	0.0(−0.07)	−0.58(−0.20)	−0.23

The DOS at VBT deserves special attention; the ~1 eV wide peak of spin-polarized Cu d_{yz} and O (p_y,p_z) states is visibly separated from the main body of the valence manifold lying below. This peak, sometimes referred to as the Zhang-Rice band, plays a crucial role in the doping mechanism since it becomes hole occupied upon doping. Clearly, the injected holes will deplete only majority states so that the overall magnetization will be reduced anyway. Furthermore, we can argue that if hole doping caused a mere peak depletion, the intrachain FM ordering would be maintained, whereas a disruption of the intrachain FM ordering would require dramatic changes in the DOS shape (the latter scenario is indeed related to the ZRS formation, as illustrated later on).

In Fig. 3 we can see the detail of the bands contributing to the VBT peak: the peak results from six double-degenerate $(d_{yz}-p_y,p_z)$ bands (for $n=3$ we have 12 CuO_2 units in the supercell, of which are six up polarized and six down polarized). These bands are quite flat almost everywhere except along the k_y-parallel directions (i.e., along the chain) where a small dispersion is visible. Notice that this remarkable flatness at VBT is not generally typical of a Mott-Hubbard insulator but is emphasized here by the one dimensionality of the system. Finally, since the system is made of FM chains in order to have a spin-conserved optical transition across the energy gap, an electron must jump into a different chain. In other words there are no empty states available for intrachain optical absorptions (at least not within 6 eV above VBT, as shown by the OR-DOS in Fig. 2).

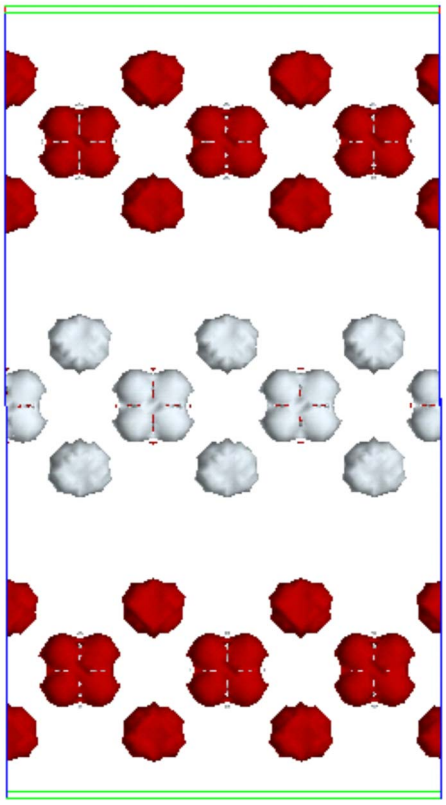

FIG. 4. (Color online) Hole spin-density isosurface for undoped CaYCuO calculated at $\rho=0.08$ bohr^{-3}. The clear (white) and dark (red) portions are for up- and down-polarized hole charges.

Finally, in Fig. 4 we plot the hole charge isosurface, i.e., the charge density for the states lying 4 eV above the VBT. From this picture we can clearly see the symmetry of the p-d hybridized state (i.e., the d_{yz} orbital and the mixture of p_y and p_z charges forming roughly circular disks) and the magnetic ordering of the system.

IV. LOW-DOPING REGION

We explored the low-doping regime $(0<x/n<1/4)$ employing $n=4$ supercell calculations and found no presence of ZRS. The essential feature is, in fact, a progressive depletion of the VBT peak as doping is increased. The hole charge is distributed (spread) all over the CuO_2 units, with each Zhang-Rice band roughly occupied by $\sim(x/n)$ holes. As already pointed out, since the depletion only involves majority states, the magnetization of a single CuO_2 unit is simply scaled down by nearly the same amount $\delta M \sim -x/n$. In Table II, which reports the orbital and site decompositions of the

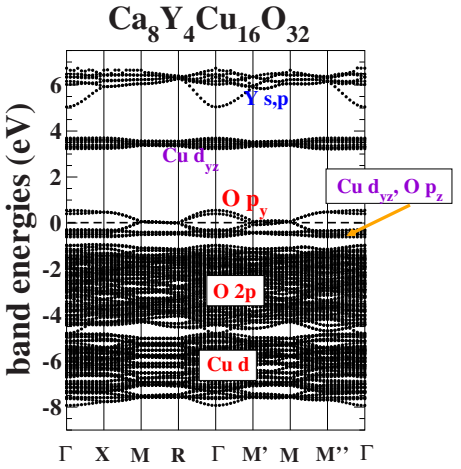

FIG. 5. (Color online) Band energies of CaYCuO for $x/n=0.25$ and $n=4$.

magnetization for all dopings studied, we see that the CuO_2 magnetization drops by $0.26\mu_B$ or over 25% between $x/n=0$ and 1/4; the intrachain magnetization indeed decreases linearly in the low-doping regime, while both intrachain FM and overall AF orderings remain unchanged.

Figures 5 and 6 show our calculated band energies and OR-DOS at $x/n=1/4$ and $n=4$ (that is, one hole every four CuO_2 units). In the band energy diagram we see that the $(d_{yz}-p_y,p_z)$ majority bands are very flat, as expected, along the k_x and k_z directions (orthogonal to the chains) corresponding to the M-R and M'-M segments of the Brillouin zone, while only a minimal dispersion of ~0.1 eV is visible along the chains (e.g., X-M or M-M'' segments). At $x/n=1/4$ the bands are cut by E_F along k_x and k_z so that the injected holes can hop across parallel chains, whereas they must be thermally activated in order to move along the

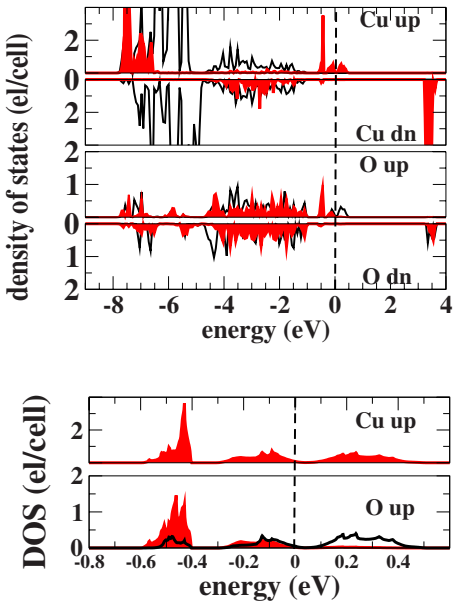

FIG. 6. (Color online) Upper panel: OR-DOS of CaYCuO for $x/n=0.25$, $n=4$. Lower panel: enlargement of majority OR-DOS around E_F. Line legend is the same as for previous OR-DOS figure.

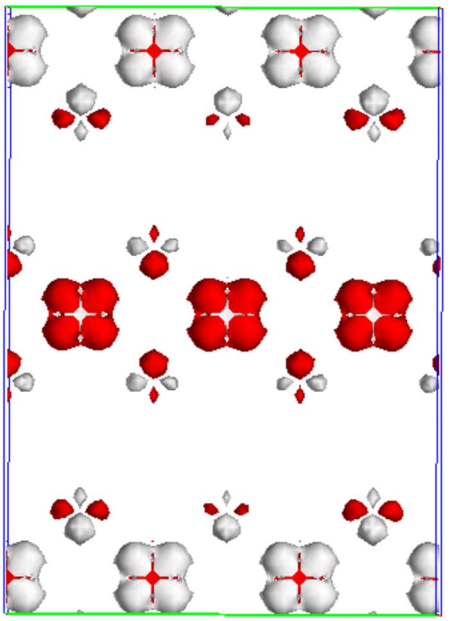

FIG. 7. (Color online) Hole spin-density isosurface ($\rho=\pm0.08$ Bohr^{-3}) for doped CaYCuO at $x/n=1/4$ for $n=4$. The clear (white) and dark (red) surfaces are for up- and down-polarized hole charges.

chains. At lower and lower x/n, E_F moves up to the top of the undoped VBT peak, thus, it intersects the bands in the chain-parallel direction as well. However, the band dispersion is so small that we can envisage hopping as the only relevant conductivity mechanism at this doping. In summary, at low doping our results suggest CaYCuO as a low-mobility hopping-conductive system in agreement with the experiments.[6]

In Fig. 6 we also report an OR-DOS blowup near E_F; it resembles that of a Coulomb gap insulator with hopping conductivity. Finally, in Fig. 7 we show the calculated hole charge isosurface. We can see that while d_{yz} hole charge shows no significant change with respect to the undoped case, some intra-atomic antiferromagnetisms show up on the oxygens. In particular, the p_z hole charge is still FM aligned to the native d_{yz} holes of the adjacent Cu, while the p_y hole charge is antialigned to the Cu holes. This is a consequence mainly of the p_y depletion visible in the lower panel of Fig. 6. We can summarize the system behavior at low doping as follows: for a small amount of injected hole charge, the Cu d-d hole repulsion is not large enough to induce the formation of stable ZRS, the hole charge spreads through the chains, and the magnetic ordering of the pure bulk system remains unchanged.

V. INTERMEDIATE REGION: APPEARANCE OF ZRS

Our calculations show that for $x/n>1/4$, the physics of CaYCuO is essentially dominated by ZRS formation, in turn, ignited by strong hole localization on the oxygens. It is quite remarkable that a band theory, such as the PSIC, can substantiate by first principles the Zhang-Rice model result. According to the Zhang-Rice picture, holes injected by doping

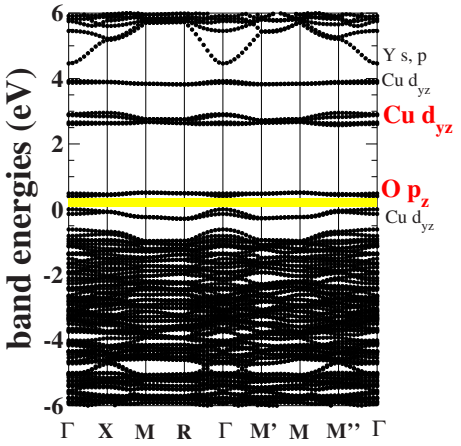

FIG. 8. (Color online) Band energies of CaYCuO at $x/n=1/3$, $n=3$. Labels in (red) bold signal ZRS-coupled bands; the others are for undopedlike bands [notice however that d_{yz} bands are really $d_{yz}-(p_y,p_z)$ hybridized bands with predominant d_{yz} character, and p_z bands are really d_{yz}-p_z hybridized bands with dominant p_z (see the OR-DOS)]. The (yellow) filled area highlights the optical gap, which opens as consequence of the ZRS formation.

within the CuO_2 units prefer to be located on the oxygens, rather than on the Cu^{2+} (d^9) sites, as a consequence of the strong Coulomb repulsion (U) between two holes sited on the same d orbital. Furthermore, as prescribed by superexchange rules, the injected hole is coupled antiferromagnetically to the native hole on the adjacent Cu^{2+} ion so that the two-hole system forms a spin-singlet state, which demagnetizes the corresponding CuO_2 unit. A large concentration of ZRS thus determines the disruption of the underlying magnetic ordering.

In Figs. 8–10 we display band energies, OR-DOS, and magnetization density, respectively, for $x/n=1/3$. At this concentration the whole doping hole charge is localized to form ZRS, and we have one ZRS, each of the three CuO_2 steps (a chain configuration that can be labeled as "-1-1-0-,"

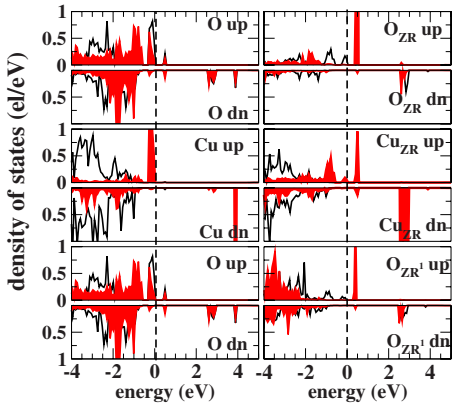

FIG. 9. (Color online) OR-DOS of CaYCuO at $x/n=1/3$, $n=3$. Legend is the same as the previous OR-DOS figures. As ZRSs are present at this doping concentration, we have unequivalent Cu and O atoms: In the right column there are atoms of ZRS CuO_2 units with strongly spin-polarized oxygens (O_{ZR}), and in the left column are atoms of FM (i.e., non-ZRS) CuO_2 units with weakly polarized oxygens.

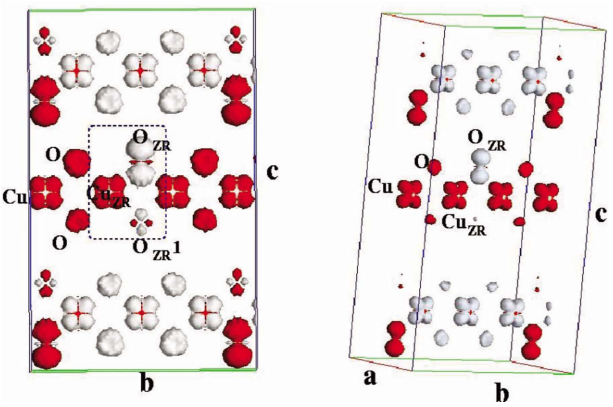

FIG. 10. (Color online) Hole spin-density isosurface for $x/n=1/3$, $n=3$. Left: on-top view of the (b,c) plane calculated at $(\rho)=\pm 0.008$ bohr^{-3}. Right: three-dimensional view at $\rho=\pm 0.027$ bohr^{-3}. The white and (red) dark surfaces show up and down-polarized contributions. The dashed box encloses a single ZRS.

where 1 and 0 indicate non-ZRS and ZRS units, and the infinite repetition of the sequence is understood). Look first at the bands: the striking feature here is the breakup of the undoped Zhang-Rice band into two essentially flat bands, one filled and the other empty, running through the entire BZ and separated by a gap $E_{pol}\sim 0.4$ eV; the system is insulating at this doping (in Fig. 8 the gap is highlighted). The empty bands at ~ 0.4 eV above the VBT represent doping-injected, oxygen-localized, and fully polarized holes of p_z symmetry (see also the OR-DOS), partially extended onto the adjacent Cu d_{yx} orbital as well. Since we have four holes in the $n=3$ unit cell (one hole per unit chain) due to the AF symmetry, we can count in the band energy diagram two double-degenerate spin-polarized empty bands at 0.4 eV. The coupling of p_z holes with native d_{yz} spin-minority holes is signaled by the ~ 1 eV energy downshift of the latter with respect to the undoped value. These two antialigned holes form the ZRS, while the spin-minority d_{yz} states not coupled to any O p_z localized hole (i.e., not engaged in ZRS) remain in the undopedlike position ~ 3.5 eV above the VBT.

The OR-DOS in Fig. 9 confirms the picture, indicating that the above mentioned bands display a fair amount of p-d hybridization. At variance with the low-doping case, now we have three markedly different kinds of oxygens. These can be better identified looking also at the corresponding hole charge density in Fig. 10. In the left panels of Fig. 9 we show the DOS projected on Cu and O atoms not involved in ZRS, while in the right panels we show ZRS-participating atoms labeled as Cu_{ZR}, O_{ZR}, and O'_{ZR}. We notice in Fig. 10 that actually the localized injected hole sits almost entirely on one specific oxygen (O_{ZR}) of the CuO_2 chain step, while the other oxygen (O'_{ZR}) only marginally reflects the presence of the ZRS through a modest p_z hole fraction antialigned to the adjacent Cu_{ZR} d_{yz} orbitals (in the isosurface at three times larger density in the right panel of Fig. 10, the contribution of O'_{ZR} indeed disappears). This can be appreciated by quantitatively considering the magnetization contribution from each single atom (and orbital) in Table II at $x/n=1/3$: we have an alternance of highly magnetized ($M=1\mu_B$) non-ZRS

CuO_2 units and ZRS units with perfect spin compensation ($M=0$) almost entirely due to only two orbitals, i.e., the Cu_{ZR} d_{yz} and O_{ZR} p_z, whereas no net contribution comes from O'_{ZR}. Furthermore, comparing the occupation numbers of $x/n=0$ and $x/n=1/3$ systems, we see that Cu_{ZR} captures 0.05 holes (it changes from 0.70 to 0.65 electrons), O_{ZR} gains 0.78 holes (from 0.13 to −0.65 electrons), and finally O'_{ZR} gains 0.13 holes (from 0.13 to 0.0 electrons). Thus the ZRS hole is distributed ~80% on O_{ZR}, ~13% on O'_{ZR}, and ~5% on Cu_{ZR}. The p_z shape of the hole suits the need for minimal overlap with the native d_{yz} hole, where the Cu-O projections along the y (chain-parallel) and z (chain-orthogonal) directions are 1.32 and 1.42 Å, respectively.

Our values for orbital occupations at $x/n=1/3$ signal an abrupt change in magnetization with respect to the low-doping regime characterized by a continuous linear decrease in M with x/n. This reflects a phase transition from magnetic order to ZRS-populated disordered array of variously magnetized CuO_2 units, which may be pictured as paramagnetic or short-range correlated behavior consistent with the smoothening of the AF susceptibility peak observed by Hayashi *et al.*[6] Notice that the overall AF symmetry visible in Fig. 10 has been retained (i.e., up-polarized and down-polarized hole charges can be exchanged by a space-group operation) for computational convenience but bears no physical significance. Once ZRSs arise, intrachain FM ordering is weakened or even completely destroyed, and the much smaller interchain coupling can be considered totally ineffective.

It is appropriate to sketch a simple argument explaining the transition from low-doping to ZRS regime. Our results suggest that the ZRS formation occurs provided that doping concentration (i.e., injected positive charge) is large enough to make the effective hole-hole Coulomb repulsion larger than some Cu-O band hybridization energy that would favor mere band depletion upon doping. We can estimate the doping threshold at which the transition occurs as follows: Our calculations give $U\sim 11$ eV and a native hole charge $\rho_n \sim 0.7$ per Cu (entirely accumulated in minority d_{yz} orbitals). We saw that at low doping roughly half of the total injected hole charge $\rho_i=x/n$ per CuO_2 goes to majority d_{yz} Cu orbitals (the other half goes to the two oxygens), so we obtain an effective hole-hole repulsion $\rho_n\rho_i U/2\sim 3.85(x/n)$ eV. This quantity becomes larger than the width of the undoped Zhang-Rice band (~1 eV, see Fig. 2) for $x/n>0.26$, which is quite consistent with our direct findings.

Notice that, according to an ideal Hubbard picture, the threshold of Zhang-Rice singlet formation corresponds to a Coulomb repulsion larger than the so-called Cu-O charge-transfer energy, i.e., the energy paid to move the injected hole from the Cu d states into the O p states, supposedly located somewhat below (or above from a hole perspective) in energy. In fact, according to our calculations the Cu-O charge-transfer energy is rather immaterial as Cu and O states largely overlap through all their (valence and conduction) energy window. Our results suggest, instead, that the parameter antagonist to the ZRS formation is the width of the Zhang-Rice band, which measures the energy paid in the process of hole charge localization.

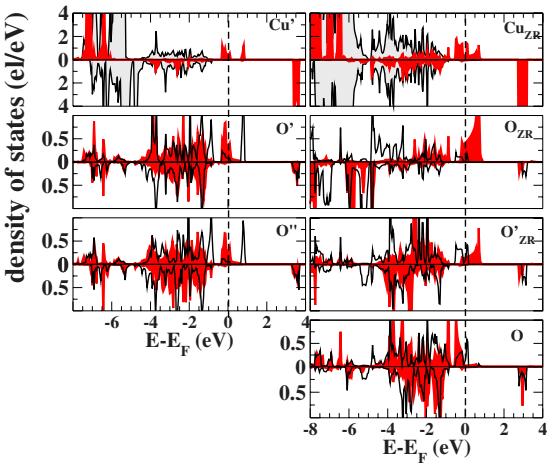

FIG. 11. (Color online) OR-DOS for CaYCuO at doping $x/n=1/2$, calculated for $n=2$ (legends is the same as that used for the other OR-DOS figures). Left panels show atoms not involved in ZRS formation; right panels show atoms within ZRS-rich chains. To trace each panel back to the corresponding atom see the hole density isosurface plot in Fig. 12.

VI. HIGHLY DOPED REGION

While experiments are only available up to $x/n=0.4$, we have performed calculations over the whole doping range up to one hole per CuO_2 ($x/n=1$). CaYCuO changes regime again around $x/n\sim 1/2$, i.e., for one hole every two CuO_2 steps on average. At this concentration another phase transition occurs: As the average hole-hole distance is reduced, ZRS show a strong tendency to line up along the same chain, rather than be isotropically scattered throughout so that the nearest-neighbor ZRSs start to overlap with each other, spreading in space and energy. This ultimately causes the collapse of the optical gap seen in the Zhang-Rice insulating region and the opening of one-dimensional conducting channels along the chains. Thus, the high-doped ($x/n>1/2$) ZRS-rich region is characterized by one-dimensional metallic (i.e., Tomonaga-Luttinger liquid) behavior.

As for magnetic ordering, for $x/n\geq 1/2$ the system appears as a mixture of "imperfect" ZRS (i.e., holes on O and Cu within a single CuO_2 unit do not exactly compensate anymore, and the ZRS magnetization may not strictly vanish) and variously magnetized CuO_2 units (in the following we still name ZRS the barely compensated CuO_2 units since they represent the natural evolution of the exact ZRS in the metallic limit).

The increase in ZRS concentration demagnetizes more and more CuO_2 units, progressively suppressing the magnetization density along the chains, but leaving Cu magnetic moments comparable to their undoped value. As will be discussed in this section, this demagnetization is not homogeneous but proceeds by orderly patterns as ZRSs prefer to line up as densely as possible along a single chain, rather than being evenly distributed through all the chains.

High-doping configurations can be conveniently evaluated using unit cells with two-step chains ($n=2$). In Figs. 11 and 12 the OR-DOS and the hole spin-density isosurface calculated for $x/n=1/2$ and $n=2$ are shown, respectively. In

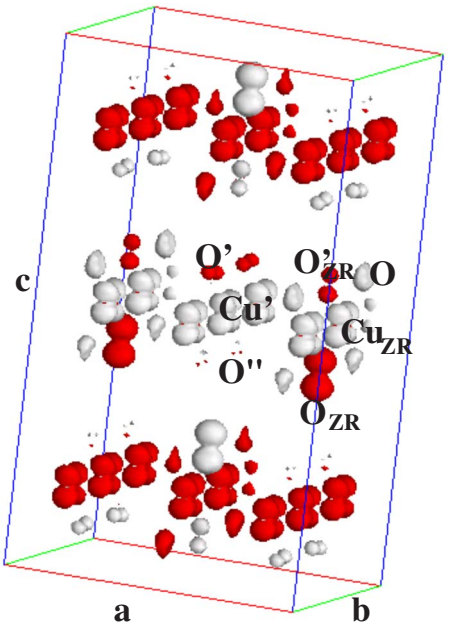

FIG. 12. (Color online) Hole spin-density isosurface calculated at value $\rho = \pm 0.027$ bohr^{-3} for the high-doping $x/n=1/2$ ($n=2$) concentration.

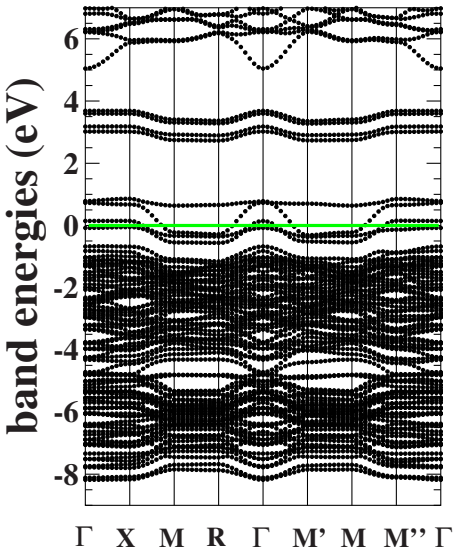

FIG. 13. (Color online) Band energies of CaYCuO calculated at $x/n=1/2$ and $n=2$.

Fig. 12 this solution is made of two different chains (each one duplicated by AF symmetry, again imposed for computational convenience): one chain has a well visible ZRS identified by the big hole of p_z symmetry on the oxygen, alternated with a non-ZRS unit (the "-1-0-" array), and another chain that is ZRS-free (a "-1-1-" sequence). Thus, we now have several inequivalent atoms; Cu_{ZR}, O_{ZR}, and O'_{ZR} participate to ZRS, while O is spin paired to the adjacent Cu_{ZR} and antipaired to O_{ZR} and O'_{ZR}. On the other hand Cu′, O′, and O″ sit on ZRS-free chains, with O′ and O″ barely magnetized. At variance with the oxygens, coppers do not differ significantly in magnetization, and indeed they all appear very similar in Fig. 12. From the orbital occupations in Table II, the ZRS magnetization is seen to be appreciably nonzero (the negative sign indicates that the sum of O_{ZR} and O'_{ZR} contributions overcomes the Cu_{ZR} magnetization that is taken with positive sign).

Focusing on the oxygens, we see in Fig. 11 that the injected holes on O_{ZR} and O'_{ZR} p_z orbitals feature an ~1-eV-wide DOS (at $x/n=1/3$ these were very narrow peaks), which span the ~0.4 eV optical gap of the $x/n=1/3$ insulating phase, thus turning the system into a metal. This occurs as the injected holes are not localized within a single CuO_2 unit, but spill out considerably on the adjacent step as well. Indeed, it can be seen in the right panels of Fig. 11 that there is remarkable hybridization between Cu_{ZR} d_{yz}, O_{ZR}, and O'_{ZR} p_z orbitals, as well as a small but visible hole charge leaking onto the adjacent O p_z orbital. This opens a conducting channel of $d_{yz}-p_z$ symmetry for spin-polarized hole current within the DOS manifold (right panels of Fig. 11).

Furthermore, due to this strong hybridization the injected hole charge captured within the ZRS chain is visibly much larger than that of the ZRS-free chain (left panels). We can see this quantitatively in Table II (the orbitals are fully spin-polarized, so hole magnetization can be equivalently thought of as hole charge): in the ZRS-rich chain, the ZRSs capture $\sim 1+0.13=1.13$ hole charges and its adjacent CuO_2 $\sim 1-0.81=0.19$ holes so that, on average, a single unit in the chain gets ~0.66 holes, which amounts to an extra contribution of 0.16 holes over the average x/n concentration. It follows that there is not enough hole charge to reproduce the same hole-rich "-1-0-" array on the other chain as well, whose CuO_2 units can only count on the remaining $x/n-0.16=0.34$ injected holes, on average. Thus in the latter the ZRS cannot form and the chain remains substantially insulating (notice that the Cu′ d_{yz} OR-DOS is gapped near E_F). The residual holes captured by O′ and O″ mainly sit on a p_y DOS peak located ~0.7 eV above E_F (see Fig. 11) and are antialigned with the holes on the adjacent Cu′. This gives rise to an intra-atomic antiferromagnetism on O′ and O″, which is well visible in the corresponding hole density of Fig. 11.

The ZRS DOS spreading is also reflected in the corresponding band structure shown in Fig. 13. Here we can see two ~1-eV-wide bands crossing E_F at two different points (k_F^1, k_F^2) along the chain direction (we have two up-polarized and two down-polarized ZRSs, which are identical by spin exchange, and each ZRS contributes one band at E_F). The corresponding Fermi surface, plotted in Fig. 14, shows the characteristic features of one-dimensional metals, i.e., parallel sheets separated by $2k_F$ vectors along the chain direction. Thus according to our calculations, we can expect the occurrence of Tomonaga-Luttinger metallic behavior at and above $x/n \sim 1/2$ concentration.

Finally, it is worth considering the possible impact on our results for $x/n=1/2$ of the $n=2$ unit cell used for the simulation. It may be argued that with larger and larger supercells (allowing for higher configurational entropy), different solutions for the electronic ground state could be obtained. In fact, while some details can depend on the overimposed boundary conditions, the main features seen for $n=2$ are ro-

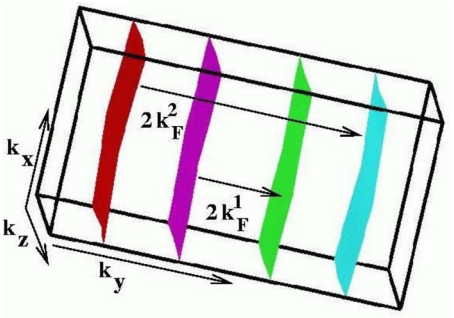

FIG. 14. (Color online) Fermi surface of CaYCuO calculated at $x/n=1/2$, $n=2$. Fermi vectors are $\mathbf{k}_F^1=0.3$ and $\mathbf{k}_F^2=0.8$ [in units of $2\pi/(b/n)$].

bust. As a proof, consider the hole density isosurfaces in Fig. 15, again for $x/n=1/2$, but calculated with $n=4$ (i.e., system $Ca_3Cu_4O_8$ with a 60-atom unit cell). In order to avoid any bias in the calculation, no point symmetry (except for the spin-exchange AF along the c axis) was included, and the starting charge for the self-consistent cycle was taken as a free-atom superposition with no relation to the $n=2$ solution. Yet, the result is very consistent with $n=2$ as we find the electronic ground state still configured as alternance of hole-rich "-1-0-" chains and lightly doped ZRS-free "-1-1-" chains.

Our results attest to the following picture: at $x/n=1/2$, ZRS cluster along a single chain, giving rise to regular array of one ZRS, each of the two CuO_2 steps. However, as the ZRSs are "impure" (i.e., $S\neq 0$) and spread onto nearby units, the "-1-0-" array requires an amount of hole charge larger than the average hole concentration (we estimate ~0.66 holes per CuO_2 as the stabilization threshold for the "-1-0-"

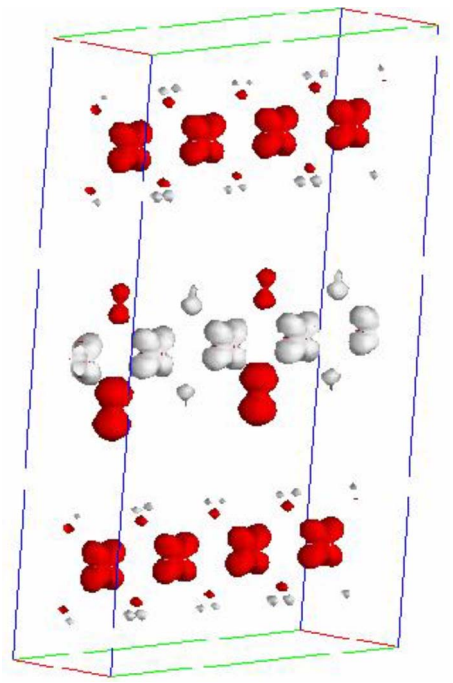

FIG. 15. (Color online) Hole spin-density isosurface calculated at $\rho=\pm 0.027$ bohr^{-3} for $x/n=1/2$ within $n=4$ supercell.

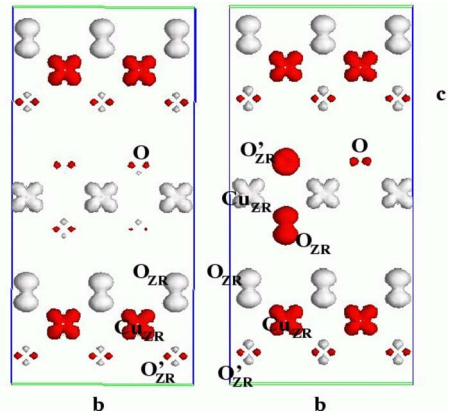

FIG. 16. (Color online) Hole spin-density isosurfaces calculated at value $\rho=\pm 0.027$ bohr^{-3} for $x/n=5/8$ (left panel) and $x/n=7/8$ (right panel) within the $n=2$ supercell.

configuration) and cannot be homogeneously replicated throughout so that some of the chains remain underdoped and ZRS poor, with oxygens residually and irregularly magnetized. We may expect that at higher doping (i.e., as soon as enough hole charge is available to condense more ZRS), the ZRS concentration will increase accordingly.

VII. VERY-HIGH-DOPING REGION

In this section we describe the characteristics of CaYCuO for doping concentrations greater than $x/n=1/2$. For brevity we will not show the detailed DOS and band energies as they appear to be similar to those already seen for $x/n=1/2$. Indeed, for $1/2<(x/n)<1$ the system maintains its one-dimensional metallic behavior, with E_F progressively shifting toward the bottom of the Zhang-Rice band. We will focus instead on a more interesting aspect, i.e., the concentration and the distribution of ZRS along the chains, which are quite sensitive to the doping concentration. The hole magnetization is displayed in Fig. 16 for $x/n=5/6$ and 7/8.

As x increases above $x/n=1/2$, the system becomes ZRS richer, i.e., ZRS formation is not inhibited but favored by higher doping. ZRSs are quite robust energetically (non-ZRS solutions do not even reach self-consistency) and their concentration rises roughly linearly with x/n. Our hole density calculation at $x/n=0.625$ ($n=2$) shows that we have again ZRS-empty "-1-1-" chains, but now they are alternated with ZRS-saturated "-0-0-" chains, i.e., chains where each Cu_2 unit hosts one ZRS. It is interesting to notice that the system prefers to be configured in this ("-0-0-" and "-1-1-") array, rather than in the more homogeneous ("-1-0-" and "-1-0-"), having the same overall ZRS concentration. This indicates a preference of ZRS to condense as much as possible along a single chain, rather than being homogeneously distributed.

At $x/n=0.75$ ($Ca_{1/2}Y_{1/2}Cu_2O_4$), we find a more complicated array, with one "-0-0-" alternated with three "-1-0-" chains (so that the average ZRS concentration is 2/3), and finally at $x/n=7/8$ we have an alternation of "-0-0" and "-1-0-" chains (thus 3/4 ZRS concentration). It is interesting to peruse Table II for the orbital magnetizations at $x/n=7/8$: We can distinguish two types of ZRS units, according

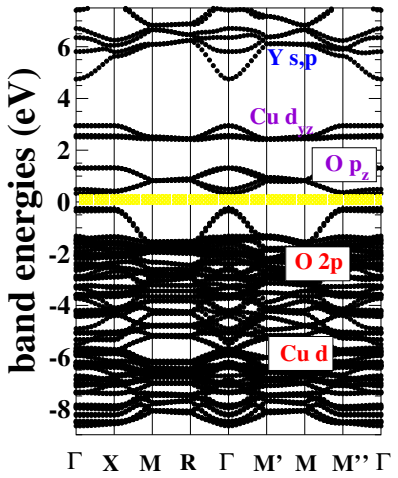

FIG. 17. (Color online) Band energies for $x/n=1$, with $n=2$.

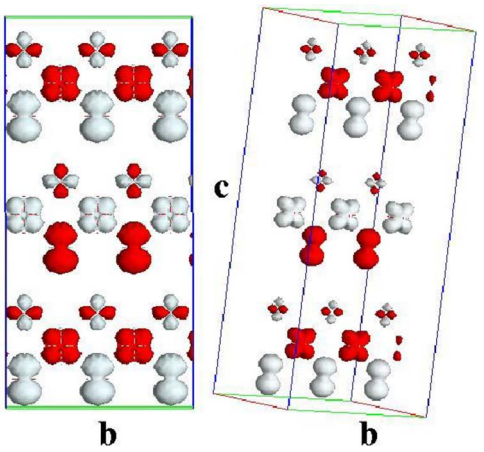

FIG. 18. (Color online) Hole spin-density isosurface for $x/n=1$, $n=2$ at $\rho=\pm 0.027$ bohr^{-3}.

to their participation in "-0-0-" or "-1-0-" chains. In the ZRS-filled chain we have two identical CuO_2 units with total magnetization of $-0.04\mu_B$ (i.e., each unit collects 1.04 holes), while in the "-1-0-" chain we have non-ZRS and ZRS alternated units with magnetizations of $0.82\mu_B$ and $-0.23\mu_B$ (thus 0.18 and 1.23 holes), respectively. This gives an average of 0.8725 holes per CuO_2, which is almost exactly the x/n value.

VIII. FULL DOPING

A further and last phase transition is reached for $x/n=1$. This is the concentration needed to completely empty the Zhang-Rice band. As we have seen that this band is well separated by the remaining valence manifold, it is not surprising that at this doping the system turns back to insulating. Figure 17 shows indeed an ~ 0.5 eV optical gap.

However, the most interesting aspect involves the magnetization. Now all the CuO_2 units are ZRS, i.e., all the chains are in a "-0-0-" configuration and a remarkably exotic ZRS-saturated insulating regime appears. The system is a collection of singlets, i.e., a potentially perfect diamagnet and magnetization vanishes exactly. However, Cu magnetic moments still remain similar to their undoped values. Our calculations for the orbital-resolved magnetization give $+0.64\mu_B$ for Cu_{ZR} d_{yz}, $+0.03\mu_B$ and $-0.67\mu_B$ for O_{ZR} p_y and p_z, and $-0.12\mu_B$ and $+0.12\mu_B$ for O'_{ZR} p_y and p_z, respectively. In the hole density isosurface plot of Fig. 18 we can appreciate the perfect ZRS alignment along all the chains. Calculations are done within the $n=2$ cell, i.e., for the 28-atom $CaCu_2O_4$ system.

IX. DISCUSSION

In this section, we briefly wrap up the properties of doped CaYCuO as determined by our first-principles calculations with the help of Fig. 19, which reports the ZRS concentration as a function of the doping concentration. First of all we can distinguish two main areas: the AF region (to the left of the figure) characterized by undopedlike magnetic ordering and hopping-conducting behavior and the ZRS region to the right. In the former phase the injected holes deplete the weakly dispersed Zhang-Rice band near the VBT and are homogeneously distributed both within and throughout the chains. Thus magnetization decreases steadily with x, and AF alignment is conserved. Due to the flatness of the bands around E_F, the system can be aptly described as a hopping conductor. Then at $x/n\sim 0.3$ the AF-ZRS phase transition occurs, characterized by a specific signature in the band structure: the detachment and the uprise of flat energy levels above the Zhang-Rice band peak due to hole localization on the oxygen sites, prefiguring transport properties dominated by optical-absorption conductivity. The low doping to ZRS phase transition must be associated to the loss of AF ordering and the rise of paramagnetic and/or spin-glass behavior, as reported by the many experimental reports carried out so far.[6–9]

We underline that to our knowledge no account of the microscopic characteristics of ZRS in one-dimensional cuprate with zigzag Cu-O-Cu structure was reported previously. According to our results, holes contributing to a ZRS

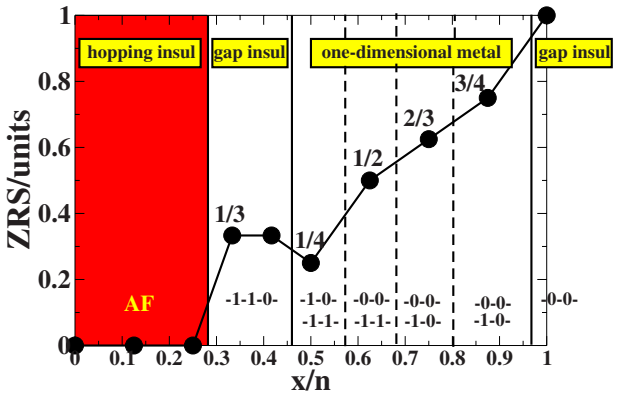

FIG. 19. (Color online) The number of ZRS per CuO_2 units as a function of hole doping x/n. The red area highlights the AF (ZRS-free) region with respect to the ZRS configurations. The solid vertical lines indicate change in envisaged conduction properties; the dashed vertical lines indicate change in ZRS configurations.

are mainly localized on a single oxygen and show a p_z-shaped symmetry. In no case did we find two holes sitting on two oxygens within the same CuO_2 unit (this agrees with the Hubbard-derived notion that two ZRS on the same CuO_2 always repel each other).

The ZRS regime displays transitions from gap insulator to one-dimensional metal at $x/n \sim 0.5$ and again to gap insulator at the end point $x/n=1$. Above $x/n=1/2$ the optical gap closes due to the spread of ZRS in space and energy. At $x/n=1$ the system is again gap insulating as the Zhang-Rice peak is now completely emptied.

As for the ZRS/CuO_2 concentration, we see a drop from 1/3 at $x/n=1/3$ to 1/4 at $x/n=1/2$, i.e., in correspondence with metal-insulating phase transition. We can understand the decrease in ZRS population in terms of different hole charge contributions to the ZRS formation, as we have seen in the metallic phase, due to the ZRS spread onto contiguous units. The amount of hole charge required to form the ZRS-rich "-1-0-" array (0.66 holes per unit) is much larger than the 0.33 holes/units needed to stablilize the "-1-1-0-" insulating chain at $x/n=1/3$.

Above the metallic threshold $x/n \sim 0.5$, the ZRS concentration follows a remarkably regular (and roughly linear) rise of x/n to $x/n=1$. The growth of ZRS concentration is characterized by several changes in the ZRS distribution patterns: ZRSs tend to regularly cluster along the chain in order to minimize their nearest-neighbor distance. Thus, with increasing hole doping the chain configuration change from "-1-1-0" at $x/n=1/3$ to "-0-0-" at $x/n=1$. The latter is a collection of singlet states (due to symmetry, now $S=0$ exactly for each CuO_2) and thus should behave as a diamagnetic system, despite large compensating Cu and O magnetizations.

The tendency to ZRS alignment suggest that segments of regularly spaced ZRS could be actually visible at low doping (e.g., below the 1/3 threshold of the ZRS appearance) simply conveying an hole fraction $\delta x/n$ onto a specific chain that would increase its hole charge by $(\delta x/n)^N$ if N is the chain number, although we may argue that long segments of ordered ZRS at low doping may be disfavored by configurational entropy.

As discussed in earlier works,[7–9] at $x/n=1/3$ a cluster-spin glass or even spin-liquid behavior due to single units or small FM segments of undoped CuO_2 chains should be expected. Furthermore, susceptibility measurements based on superconducting quantum interference device[9] suggest the possible formation of more structured patterns of ZRS distributions in the chains. Exploration of these inhomogeneities with our calculation would require symmetries larger than the four-chain supercells used in this work and are out of reach of current computing capabilities. More complicated ZRS patterns may affect not so much the overall picture but detailed features, such as the optical gap value in the ZRS regime ($\sim$0.4 eV according to our calculations and $\sim$0.1 eV according to the experiments). However, the experimental value is measured for polycrystals, and a discrepancy with our result may be expected.

X. CONCLUSIONS

In conclusion, CaYCuO is an amazingly variegated system whose properties crucially depend on the hole doping concentration. Since doping manipulation can induce phase transitions in magnetic and conducting properties, this system is an ideal benchmark for the study of metal-insulating transitions in one-dimensional Mott insulators. In this paper, we delivered a microscopic *ab initio* account of the basic properties of CaYCuO as a function of hole doping through the whole doping range (well above the current experimental limits). In particular, we described the general characteristics of ZRS formation in one-dimensional cuprates with zigzag-shaped Cu-O-Cu bonds and their impact on magnetic and conductive properties. This result greatly encourages the application of the method to generic cuprates, although investigation of more structurally complicated materials (such as bidimensional high-T_c superconductors) would require larger unit cells and heavier computing tasks in order to explore a significant sample of electronic and structural configurations.

ACKNOWLEDGMENTS

A.F. acknowledges MIUR project "Cervelli per la ricerca" for financial support. This work was supported in part by MIUR through PON-CyberSar and PRIN 2005 projects. The calculations were performed on the SLACS-HPC cluster at CASPUR Rome.

[1] For a review, see, e.g., P. W. Anderson, P. A. Lee, M. Randeria, T. M. Rice, N. Trivedi, and F. C. Zhang, J. Phys.: Condens. Matter **16**, R755 (2004), and references therein.

[2] P. W. Anderson, Science **235**, 1196 (1987).

[3] Y. Mizuno, K. Tsutsui, T. Tohyama, and S. Maekawa, Phys. Rev. B **62**, R4769 (2000).

[4] M. Ashida, T. Ogasawara, Y. Tokura, S. Uchida, S. Mazumdar, and M. Kuwata-Gonokami, Appl. Phys. Lett. **78**, 2831 (2001).

[5] F. C. Zhang and T. M. Rice, Phys. Rev. B **37**, 3759 (1988).

[6] A. Hayashi, B. Batlogg, and R. J. Cava, Phys. Rev. B **58**, 2678 (1998).

[7] H. F. Fong, B. Keimer, J. W. Lynn, A. Hayashi, and R. J. Cava, Phys. Rev. B **59**, 6873 (1999).

[8] M. Matsuda, H. Yamaguchi, T. Ito, C. H. Lee, K. Oka, Y. Mizuno, T. Tohyama, S. Maekawa, and K. Kakurai, Phys. Rev. B **63**, 180403(R) (2001).

[9] M. D. Chabot and J. T. Markert, Phys. Rev. Lett. **86**, 163 (2001).

[10] E. Dagotto, Rev. Mod. Phys. **66**, 763 (1994).

[11] S. R. White and D. J. Scalapino, Phys. Rev. B **61**, 6320 (2000).

[12] A. Filippetti and N. A. Spaldin, Phys. Rev. B **67**, 125109 (2003).

[13] A. Filippetti and V. Fiorentini, Phys. Rev. Lett. **95**, 086405 (2005).

[14] A. Filippetti, and V. Fiorentini, Phys. Rev. B **74**, 220401(R) (2006).

[15] A. Filippetti and V. Fiorentini, Phys. Rev. Lett. **98**, 196403 (2007).
[16] A. Filippetti and V. Fiorentini, J. Magn. Magn. Mater. **310**, 1648 (2007).
[17] A. Filippetti, G. M. Lopez, M. Mantega, and V. Fiorentini arXiv:0803.0484 (unpublished).
[18] A. Svane and O. Gunnarsson, Phys. Rev. Lett. **65**, 1148 (1990).
[19] M. Stengel and N. A. Spaldin, Phys. Rev. B **77**, 155106 (2008).
[20] D. Vanderbilt, Phys. Rev. B **41**, 7892 (1990).